



**HAL**  
open science

## A transcriptomic roadmap to $\alpha$ - and $\beta$ -cell differentiation in the embryonic pancreas

Léon van Gulp, Mauro Muraro, Tim Dielen, Lina Seneby, Gitanjali Dharmadhikari, Gérard Gradwohl, Alexander van Oudenaarden, Eelco de Koning

► **To cite this version:**

Léon van Gulp, Mauro Muraro, Tim Dielen, Lina Seneby, Gitanjali Dharmadhikari, et al.. A transcriptomic roadmap to  $\alpha$ - and  $\beta$ -cell differentiation in the embryonic pancreas. *Development* (Cambridge, England), 2019, 146 (12), pp.dev173716. 10.1242/dev.173716 . inserm-02438309

**HAL Id: inserm-02438309**

**<https://inserm.hal.science/inserm-02438309v1>**

Submitted on 14 Jan 2020

**HAL** is a multi-disciplinary open access archive for the deposit and dissemination of scientific research documents, whether they are published or not. The documents may come from teaching and research institutions in France or abroad, or from public or private research centers.

L'archive ouverte pluridisciplinaire **HAL**, est destinée au dépôt et à la diffusion de documents scientifiques de niveau recherche, publiés ou non, émanant des établissements d'enseignement et de recherche français ou étrangers, des laboratoires publics ou privés.

# A transcriptomic roadmap to $\alpha$ - and $\beta$ -cell differentiation in the embryonic pancreas

Léon van Gurp<sup>1,\*</sup>, Mauro J. Muraro<sup>1,2,\*</sup>, Tim Dielen<sup>1</sup>, Lina Seneby<sup>1</sup>, Gitanjali Dharmadhikari<sup>1</sup>, Gerard Gradwohl<sup>3</sup>, Alexander van Oudenaarden<sup>1,2,4</sup> and Eelco J. P. de Koning<sup>1,5,†</sup>

## ABSTRACT

During pancreatic development, endocrine cells appear from the pancreatic epithelium when *Neurog3*-positive cells delaminate and differentiate into  $\alpha$ -,  $\beta$ -,  $\gamma$ - and  $\delta$ -cells. The mechanisms involved in this process are still incompletely understood. We characterized the temporal, lineage-specific developmental programs during pancreatic development by sequencing the transcriptome of thousands of individual pancreatic cells from E12.5 to E18.5 in mice, and identified all known cell types that are present in the embryonic pancreas, but focused specifically on  $\alpha$ - and  $\beta$ -cell differentiation by enrichment of a MIP-GFP reporter. We characterized transcriptomic heterogeneity in the tip domain based on proliferation, and characterized two endocrine precursor clusters marked by expression of *Neurog3* and *Fev*. Pseudotime analysis revealed specific branches for developing  $\alpha$ - and  $\beta$ -cells, which allowed identification of specific gene regulation patterns. These include some known and many previously unreported genes that appear to define pancreatic cell fate transitions. This resource allows dynamic profiling of embryonic pancreas development at single cell resolution and reveals novel gene signatures during pancreatic differentiation into  $\alpha$ - and  $\beta$ -cells.

**KEY WORDS:** Single cell transcriptome sequencing, Pancreas development, Alpha cells, Beta cells, *Neurog3*, Endocrine progenitors

## INTRODUCTION

Mouse pancreatic development is characterized by two main differentiation phases: the primary and secondary transition. The secondary transition, which is characterized by segregation of the pancreatic epithelium into ductal tip and trunk domains, takes place between approximately embryonic age (E) 12.5 and E15.5 (Zhou et al., 2007; Pan et al., 2013), and gives rise to the pancreatic cell types as they appear in the adult organism. The tip domain contains a population of multi-potent progenitors, expressing markers such as *Ptf1a*, *Hnf1b* and *Pdx1*, which contribute to all adult pancreatic cell types (Larsen et al., 2017; Pan and Wright, 2011). In the trunk

domain, lateral inhibition by Notch signals such as *Hes1* determines which cells will differentiate into mature ductal cells or endocrine cells (Magenheim et al., 2011; Shih et al., 2012; Kim et al., 2015).

Endocrine differentiation is marked by the appearance of neurogenin 3 (*Neurog3*), a key transcription factor during this process (Gu et al., 2002). After expression of *Neurog3*, endocrine progenitors delaminate from the ductal lining to form the islets of Langerhans in the mesenchyme surrounding the pancreatic epithelium (Seymour et al., 2007; Grapin-Botton et al., 2015). These endocrine progenitors, which stop proliferation after commitment to the endocrine lineage (Miyatsuka et al., 2011), make endocrine fate choices based on the expression of a number of key transcription factors. An early fate choice is determined by the balance in expression between mutually inhibitory genes *Pax4* or *Arx*, which push cells towards an  $\alpha$ -,  $\beta$ - or  $\delta$ -cell phenotype (Collombat et al., 2005, 2003; Sosa-Pineda et al., 1997). Although some of these important key transcription factors have been identified, the changes in regulatory gene networks during endocrine fate transitions are incompletely understood and can only be resolved at a single cell level.

Single cell transcriptomics is a recent but now popular approach that provides transcriptome-wide gene expression information from individual cells (Kolodziejczyk et al., 2015; Grün et al., 2015; Grün and van Oudenaarden, 2015). The strongest advantages over traditional bulk sequencing are the possibility of investigating gene expression patterns for each cell type individually, the ability to probe heterogeneity within cells of the same type and the ability to identify rare cell types within a population. We and others have recently analyzed gene expression in adult human and murine pancreatic tissue at the single cell level (Muraro et al., 2016; Segerstolpe et al., 2016; Baron et al., 2016; Xin et al., 2016; Wang et al., 2016; Lawlor et al., 2017; Li et al., 2016; Xin et al., 2018; Fang et al., 2019). In addition, other studies have investigated differentiation processes of iPS cells and pancreatic ontogeny at the single cell level (Byrnes et al., 2018; Petersen et al., 2017; Stanescu et al., 2017; Krentz et al., 2018; Veres et al., 2019) using tools that provide a pseudo-temporal signature to order cells in developmental time (Qiu et al., 2017b,c). These studies show how single pancreatic progenitor cells develop into characteristic endocrine and exocrine cells, and how adult pancreatic cells can be minutely characterized based on gene expression profiles into  $\alpha$ ,  $\beta$ ,  $\gamma$ ,  $\delta$ ,  $\epsilon$ , ductal and acinar cell clusters. Heterogeneity within these clusters of adult cells has been detected and has allowed the identification of rare subpopulations of cells (Muraro et al., 2016; Segerstolpe et al., 2016; Wang et al., 2016).

Here, we have used SORT-seq (Muraro et al., 2016), a high-throughput single-cell mRNA sequencing pipeline that provides high-quality single cell transcriptome profiles to sequence individual GFP-positive and -negative cells from MIP-GFP mice at multiple time points during the secondary transition of murine

<sup>1</sup>Hubrecht Institute/KNAW and University Medical Center Utrecht, Uppsalalaan 8, 3584CT Utrecht, The Netherlands. <sup>2</sup>Single Cell Discoveries, 3584CT Utrecht, The Netherlands. <sup>3</sup>Institut de Génétique et de Biologie Moléculaire et Cellulaire, Université de Strasbourg, BP10142 Strasbourg, France. <sup>4</sup>Oncode Institute, 3521AL Utrecht, The Netherlands. <sup>5</sup>Department of Internal Medicine, Leiden University Medical Center, 2333ZA Leiden, The Netherlands.

\*These authors contributed equally to this work

†Author for correspondence (e.koning@hubrecht.eu)

© L.v.G., 0000-0002-6281-5964; L.S., 0000-0003-1798-3413; G.G., 0000-0002-6730-2615; E.J.P.d.K., 0000-0002-1232-7022

pancreatic development. All cells were combined into a single dataset, and divided into separate clusters representing all cell types of the embryonic pancreas using Seurat (Butler et al., 2018) and Monocle2 (Qiu et al., 2017b,c). This dataset was used to follow tissue maturation through time, to characterize progenitor cells at different stages of endocrine differentiation, to identify the distinct endocrine cell types of the pancreas that arise from these progenitors and to reveal dynamic expression of genes involved in these fate choices. This resource, which can also be easily accessed online (singlecellpancreas.eu), will provide a valuable starting point for further analysis into the function of the genes involved in the development of pancreatic cell types, especially for  $\alpha$ - and  $\beta$ -cells.

## RESULTS

### Transcriptome profiling of single cells from different developmental time points identifies all known pancreatic cell types

We set out to build a resource with which we could follow pancreatic development at the single cell resolution, and that would cover developmental stages from the second transition to birth. To ensure we captured all cell types present in the developing pancreas, we used a MIP-GFP reporter mouse that would allow us to enrich for cells with an active insulin promoter. GFP-positive and ungated embryonic pancreatic cells of embryonic ages E12.5, E13.5, E14.5, E15.5 and E18.5 were sorted independently (Fig. S1A) and processed using the SORT-seq protocol (see Materials and Methods) to later be combined into a single dataset that contains all pancreatic cell types.

After sequencing, we obtained a dataset of 7296 single cells. A total of 4620 cells remained after quality control filtering (Fig. S1C,D). Unsupervised clustering revealed 14 clusters. Differential expression analysis allowed us to classify these clusters into eight different cell types: pancreatic tip and trunk epithelium, endocrine progenitors, maturing  $\alpha$ - and  $\beta$ -cells, mesenchymal cells, immune cells and blood vessel cells (Fig. 1A,B). Cells that were sorted by MIP-GFP expression were mainly found in the endocrine cell types (endocrine progenitors, maturing  $\alpha$  cells and maturing  $\beta$  cells). Some GFP-positive cells could also be found in the mesenchymal and immune cell populations, probably due to high autofluorescence (Fig. 1C). Characterization of fluorescence intensity showed that non- $\beta$  endocrine cells had an elevated GFP intensity compared with tip and trunk epithelial cells [14.1 arbitrary units (au) for tip/trunk, 32.7 au for non- $\beta$  endocrine cells,  $P=2.1 \times 10^{-15}$ ], while cells with a  $\beta$ -cell fate expressed GFP at still much higher intensities (32.7 au for non- $\beta$  endocrine cells, 369.9 au for  $\beta$  cells,  $P=2.2 \times 10^{-16}$ ) (Fig. S1B). Typical markers, like *Gcg* and *Ins2* for  $\alpha$ - and  $\beta$ -cells, *Cpa1* and *Sox9* for tip and trunk epithelium, *Neurog3* for endocrine progenitors, *Colla1* for mesenchyme, *ApoE* for immune cells and *Cdh5* for blood vessel cells, were expressed in their specific populations (Fig. 1D), and expression of the top differentially expressed genes per cell type were mostly cell-type specific (Fig. 1E).

Next, the dataset was purified to contain only cells with a pancreatic epithelial or endocrine cell fate (see Materials and Methods). This final subset of the data contained 2589 cells, with a median of 17,429 unique transcripts and 5053 genes per cell. Of these cells, 1844 cells were sorted as GFP positive and 745 cells were sorted in an ungated manner (Table S1).

Shared nearest neighbor (SNN)-based clustering of these cells revealed nine unique clusters (Fig. 2A,B, Table S1). Genes such as *Cpa1*, *Sox9*, *Neurog3*, *Fev*, *Gcg*, *Ins2*, *Ppy* and *Sst*, which have been described to mark specific populations in the developing pancreas,

also marked specific clusters in our dataset (Fig. 2C). Based on differential expression analysis, these clusters were identified as epithelial tip (clusters 2 and 3), epithelial trunk (cluster 6), endocrine precursors (clusters 4 and 5),  $\alpha$  lineage (clusters 8 and 9) or  $\beta$  lineage (clusters 1 and 7). Analysis of the most differentially expressed genes in each cluster shows a clear cell type-specific gene signature, where differences between clusters that mark the same cell type were much more subtle (Fig. 2D). We provide the complete list of these genes as a resource that can be mined for cell type-specific genes important for embryonic pancreas development (Table S2).

Clusters of poly-hormonal cells were not identified. However, we set out to manually investigate the occurrence of multi-hormonal cells within the clusters. Hormone-expressing cells were defined as cells that expressed more than four log-normalized counts of a given hormone (see Materials and Methods; Fig. S3A). Polyhormonality was defined as any cell that expressed more than one hormone above this threshold. Seven-hundred and forty-four *Ins2*-expressing cells were mostly found in  $\beta$ -cell clusters 1 and 7, while the 535 *Gcg*-expressing cells were mostly found in clusters 8 and 9 (Fig. S3B). Only six *Ppy*- and 19 *Sst*-expressing cells were detected, and these cells were mostly found dispersed throughout the  $\alpha$ - and  $\beta$ -cell clusters (Fig. 2C). Mean hormone expression levels per cluster followed the same trend, with the highest *Ins2* expression levels in clusters 1 and 7 and the highest *Gcg* expression in cluster 8 and 9 (Fig. S3C). In total, 36 polyhormonal cells (representing 2.7% of all hormone expressing cells) were detected in the dataset. The most common combinations were cells co-expressing both *Gcg* and *Ins2* (16 cells), *Ins2* and *Ppy* (six cells), and *Ins2* and *Sst* (six cells) (Fig. S3D).

As previously described (Marty-Santos and Cleaver, 2016; Krentz et al., 2017), cell cycle stages calculated for each cell indicated that most cells from the tip and trunk domain were in either S, G2 or M phase of the cell cycle. In contrast, almost all cells within the endocrine lineages have exited the cell cycle, with only few proliferative cells still present in *Neurog3*-expressing endocrine progenitor cluster 5 (Fig. S2C and Table S1).

We used cells originating from different experiments and embryonic ages within the dataset (Fig. S2A,B). To appreciate contribution of specific embryonic ages to each cell type, we traced the number of cells within each cluster back to the embryonic age it was collected from (Fig. S2E). We noticed that cells in the epithelial tips (clusters 2 and 3) predominantly originate from E15.5, whereas endocrine progenitors (cluster 5) originate from embryonic ages E12.5-E15.5, but no longer contribute at E18.5. Then, a large percentage of  $\alpha$  cells (clusters 8 and 9) originates from embryonic age E12.5, whereas  $\beta$ -cells (clusters 1 and 7) originate largely from later embryonic ages (E15.5 and E18.5). We anticipate that it is in part due to our enrichment for MIP-GFP-expressing cells, especially as we observe that *Ins2* expression in  $\beta$ -cells is increased at later embryonic ages, likely also increasing GFP specificity for  $\beta$  cells (Fig. 2C; Fig. S2B,D). Taken together, these data validate our experimental approach to follow the dynamic gene expression changes during pancreas development, to look for novel subpopulations of cells and to analyze which gene expression patterns are important during the transition from early, undifferentiated cell types to more mature, adult-like cell states.

### Epithelial tip cells, endocrine precursors and developing $\alpha$ - and $\beta$ -cells contain heterogeneous transcriptomic signatures

Next, we characterized the pancreatic cell types as described in Fig. 2 in more detail. Unsupervised clustering designated multiple

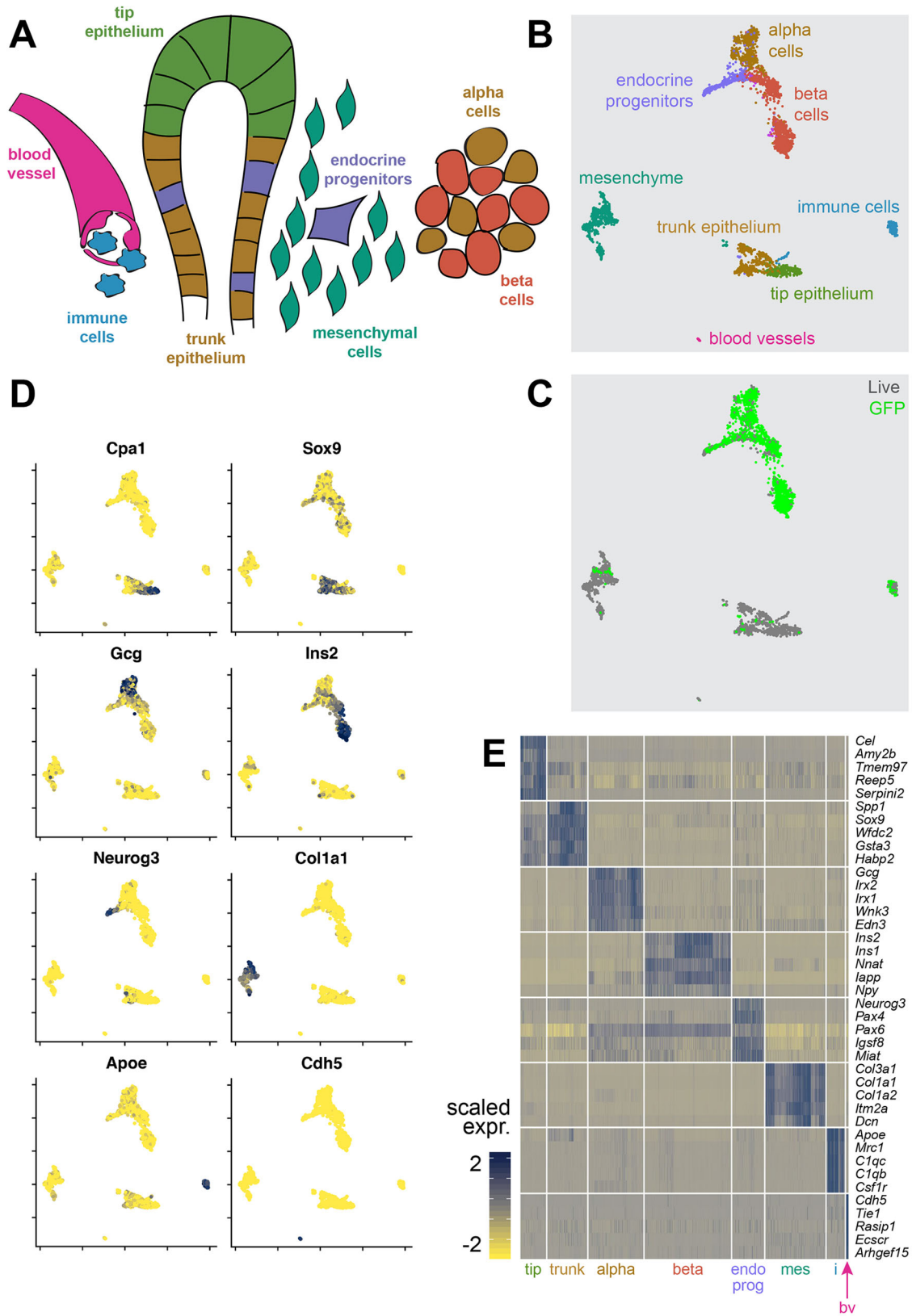


**Fig. 1. Transcriptome data from embryonic pancreatic cells of multiple embryonic ages were merged into a comprehensive dataset.** (A) A simplified schematic overview of the different cell types in the developing pancreas. Colors are matched with B. (B) A UMAP plot of all cells. Specific cell types are indicated by color, similar to A. (C) A UMAP plot of all cells. Colors indicate whether cells were live sorted or sorted as GFP-positive cells. (D) Expression maps showing log-normalized expression of typical markers for each cell type (*Cpa1*, *Sox9*, *Gcg*, *Ins2*, *Neurog3*, *Col1a1*, *Apoe* and *Cdh5*). Data are shown as log-normalized expression. Blue indicates high expression, yellow indicates low expression. (E) A heatmap showing the top five differentially expressed genes per cell type. Data are shown as scaled expression (ranging from -2 to 2). Blue indicates high expression, yellow indicates low expression. tip, tip epithelium; trunk, trunk epithelium; alpha,  $\alpha$ -cells; beta,  $\beta$ -cells; endo prog, endocrine progenitors; mes, mesenchyme; i, immune cells; bv, blood vessels.

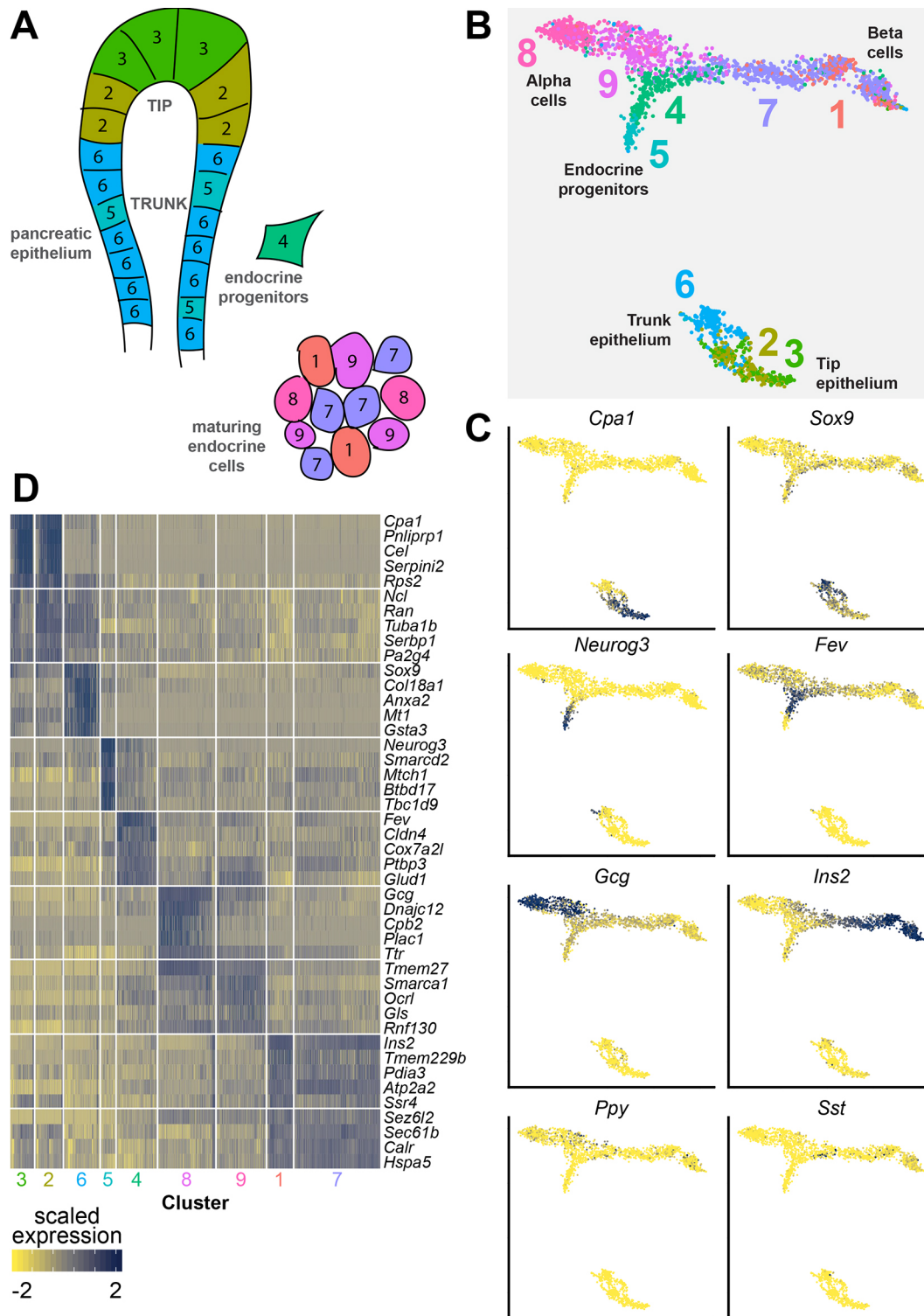


**Fig. 2.** Transcriptome data from embryonic pancreatic cells of multiple embryonic ages were merged into a subset of the complete dataset containing clusters that represent all cell types of endocrine and exocrine pancreatic cell development. (A) A simplified schematic overview of the different cell types in this subset of the developing pancreas. Colors match the UMAP in B. (B) A UMAP overview of all clustered cells in the dataset. Colors and numbers indicate clusters. (C) Expression maps showing log-normalized expression of typical markers in the developing pancreas (*Cpa1*, *Sox9*, *Neurog3*, *Fev*, *Gcg*, *Ins2*, *Ppy* and *Sst*). Data are shown as log-normalized expression. Blue indicates high expression, yellow indicates low expression. (D) A heatmap showing the top five differentially expressed genes per cluster. Data are shown as scaled expression (ranging from  $-2$  to  $2$ ). Blue indicates high expression, yellow indicates low expression.

clusters for epithelial tip cells (clusters 2 and 3), endocrine precursors (clusters 4 and 5), cells that develop an  $\alpha$ -cell signature (clusters 8 and 9) and cells that are progressing towards a  $\beta$ -cell fate

(clusters 1 and 7). We therefore asked what gene signatures are related to this heterogeneity within each of these four cell types. To answer this, we analyzed the differentially expressed genes between

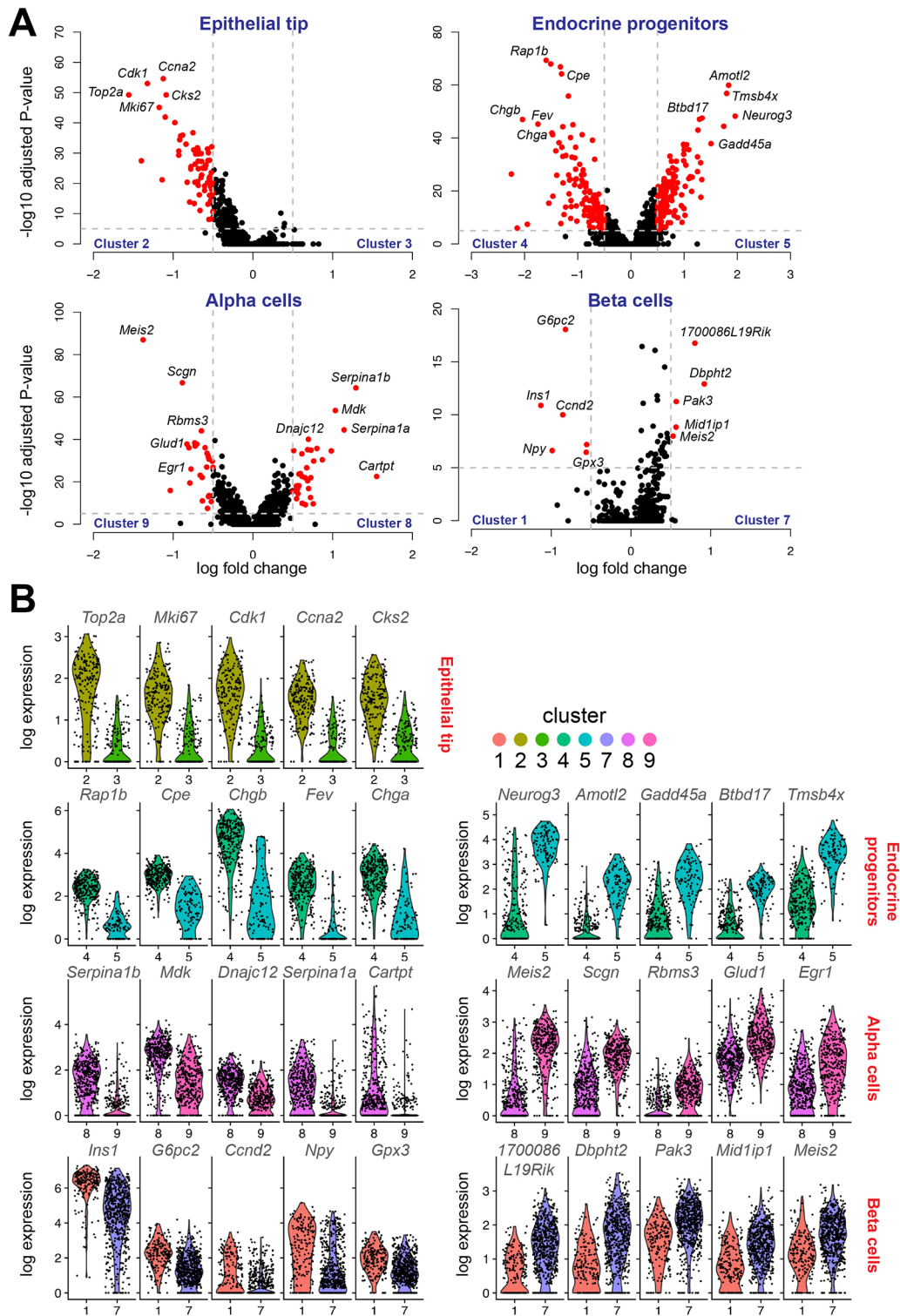


**Fig. 3. Heterogeneity within specific cell types in the developing pancreas.** (A) Differential expression was calculated for each cell type that consisted of more than one cluster, and plotted as a volcano plot (log fold change versus  $-\log_{10}$  adjusted  $P$ -value): the epithelial tip cells (clusters 2 and 3), endocrine progenitors (clusters 4 and 5),  $\alpha$ -cells (clusters 8 and 9) and  $\beta$ -cells (clusters 1 and 7). Red dots represent genes that are considered significant, with a Bonferroni corrected  $P < 1 \times 10^{-5}$  and a log fold change of at least 0.5. These thresholds are indicated by the dotted gray lines. (B) Distribution of expression of five top differentially expressed genes from clusters compared in the volcano plots in A. For cells from the tip domain (epithelial tip) only the five differentially expressed genes upregulated in cluster 2 were plotted because no significantly upregulated genes were identified in cluster 3. The violin plots are color coded in the same way as the UMAP plot in Fig. 2B for clarity. Expression on the y-axis represents log-normalized expression values. Cluster numbers are indicated on the x-axis.

the two clusters that mark the same cell type (Fig. 3A). The heterogeneity within the epithelial tip cells was mostly defined by genes that are involved in cell cycle progression, such as *Cdk1*,

*Top2a* and *Mki67* (Fig. 3A). These genes were expressed at much higher levels in cluster 2, a tip epithelium cluster found between trunk and more acinar-like tip cells in cluster 3 (Fig. 3B)

(Kowalczyk et al., 2015). Although *Hnf1b* is not differentially expressed in the pancreatic tip clusters, this gene is closely linked to both proliferation and multipotency during lineage specification (De Vas et al., 2015), leading us to believe that the heterogeneity in the tip is marked by populations of proliferative multipotent progenitors, and non-proliferating unipotent tip cells with an acinar lineage.

We also found two clusters containing endocrine precursor cells. One expressed high levels of *Neurog3* (cluster 5), which we designate as endocrine progenitors, whereas the other (cluster 4) expressed high levels of endocrine markers such as *Chga*, *Chgb* and *Cpe* (Fig. 3A-B), indicating that these cells are more specialized towards an adult endocrine cell fate. This transitory endocrine progenitor cluster (cluster 4) was specifically marked by the gene *Fev*, while the *Neurog3*-expressing cluster harbored many highly specific but unknown markers such as *Amotl2*, *Btd17* and *Gadd45a* (Fig. 3A,B). *Fev* has recently been found in another single-cell transcriptomics study of the developing pancreas that encompassed one of the embryonic ages used in our study (Byrnes et al., 2018), confirming our results that this could represent an intermediate cell state between endocrine progenitors and more-mature endocrine cell types. To further elucidate the difference between the two clusters, we performed gene ontology (GO) and gene-set enrichment (GSEA) analyses. The top five ranked GO terms associated with *Neurog3*-expressing cluster 5 were all associated with endocrine or nervous development (Fig. S4A). Alternatively, GSEA revealed a strong role for protein synthesis in *Neurog3*-expressing cells, with eight of the top 10 pathways associated with transcription, translation and ribosomes (Fig. S4C). For the transitory endocrine progenitor cluster 4, GO and GSEA were more consistent, with both analyses showing pathways related to the processing, regulation and secretion of hormones (Fig. S4B, D). This indicates that these cells resemble a more endocrine-committed, but not yet mature,  $\alpha$ - or  $\beta$ -cell-specific phenotype.

In developing  $\alpha$ - and  $\beta$ -cells, differential expression analysis of the different clusters yielded relatively few markers. In  $\alpha$ -cells, *Meis2*, *Scgn* and *Glud1* marked cluster 9, while *Serpina1a*, *Serpina1b* and *Cartpt* are markers for cluster 8 (Fig. 3B). In developing  $\beta$  cells, *Meis2*, *Pak3* and *Dbpht2* are markers for cluster 7. *Ins1*, *G6pc2* and *Npy* are highly expressed in cluster 1 (Fig. 3B). All cluster 1 genes can be linked to adult  $\beta$ -cell function. *Npy* has a role in appetite sensing and *G6pc2* is a catalytic gene, both of which have been linked to insulin secretion (Imai et al., 2007; Pound et al., 2013), while *Ins1* is related to *Ins2* and thus represents mature  $\beta$ -cell functioning. The gene profiles allowed us to characterize cluster 7 as an early and cluster 1 as a more-differentiated  $\beta$ -cell population. Similarly, cluster 9 was characterized as an early and cluster 8 as a more-differentiated  $\alpha$ -cell population. Interestingly, the gene *Meis2* is indicated in heterogeneity of both the developing  $\alpha$ - and  $\beta$ -cells. This gene has been shown to bind the pancreatic transcription factor *Pdx1* and is therefore an interesting candidate to study in the context of  $\alpha$ - and  $\beta$ -cell identity (Schnuriger et al., 2009).

In short, we found heterogenous gene signatures in several populations of the developing embryonic pancreas.  $\alpha$ - and  $\beta$ -cells split into early and late clusters. The tip epithelium can be split into a more unipotent acinar-like population and an actively dividing population that represents the multipotent tip progenitors. Finally, we found two populations of endocrine precursors: an early progenitor cluster that expresses *Neurog3* with mostly unknown endocrine progenitor marker genes. The second cluster contains cells that we consider to be transitory endocrine progenitors, have not clearly committed towards either  $\alpha$  or  $\beta$  cell fate, but express high levels of genes that are generally involved in endocrine fate

commitment, such as *Chgb* and *Fev*. This cluster could represent an intermediate cell state between *Neurog3*-positive endocrine progenitors and more mature endocrine cells (Byrnes et al., 2018).

### Pseudotime analysis reveals specific gene regulation patterning during pancreatic ontogeny

After characterizing the differences between clusters belonging to the same cell type, and identifying gene signatures that characterize early and late progenitors, we aimed to identify the genes that were differentially regulated in cells progressing from the multipotent tip through an endocrine progenitor state towards either an  $\alpha$ - or  $\beta$ -cell fate. Therefore, we performed pseudotime trajectory analysis as this allowed us to describe dynamic gene expression patterns in more detail than is possible through differential gene expression analysis, and it allowed us to evaluate cell fate plasticity over developmental time.

Cells were ordered in pseudotime and plotted in a branching trajectory using Slingshot (Street et al., 2018) and Monocle2 (Qiu et al., 2017c) (Fig. 4A, Fig. S5A-C). Slingshot, which orders cells based on original clustering, ordered cells starting at the tip epithelium (clusters 2 and 3), going through trunk epithelium (cluster 6) towards endocrine precursors (clusters 4 and 5) and branching into either an  $\alpha$ - (clusters 8 and 9) or  $\beta$ -cell fate (clusters 1 and 7). We found some inconsistencies regarding current understanding of  $\alpha$ - and  $\beta$ -cell development (Fig. S5A-C). First, the trajectory starts with cluster 3, containing multipotent tip cells, then includes cells we designated as unipotent tip cells (cluster 2), which can obviously not contribute to endocrine specification (Pan et al., 2013). Second, endocrine progenitors were only recognized to be involved in  $\beta$ -cell development, not  $\alpha$ -cell development, while lineage tracing of *Neurog3*-expressing cells indicates all endocrine cell types as descendants of endocrine progenitors (McGrath et al., 2015). Lack of recognition of endocrine progenitor cells in the development of  $\alpha$ -cells might be biased by the early timepoint of origin of the captured cells with an acquired  $\alpha$ -cell fate (Johansson et al., 2007). Finally, the branching point was determined in  $\alpha$ -cell-related cluster 9, not in one of the precursor clusters, suggesting that  $\beta$ -cell differentiation proceeds through a transient  $\alpha$ -cell-like state, while both fates are considered to be independent (Qiu et al., 2017a). In Monocle2, cells were organized from the ductal epithelium through endocrine progenitors to a branching point, after which  $\alpha$ -cell and  $\beta$ -cell specification were separated into independent branches. This was confirmed by expression of common markers *Cpa1*, *Neurog3*, *Gcg* and *Ins2* (Fig. 4A), a superimposition of the clustering analysis we performed on the pseudotime trajectory (Fig. S5D) and inversely, the superimposition of the pseudotime values on the UMAP plot of the subset of our data containing all epithelial and endocrine cells (Fig. S5E). Ordering of clusters can then be performed by looking at the distribution of pseudotime within each cluster, showing epithelial clusters first, then *Neurog3*-expressing progenitors, *Fev*-expressing transient endocrine precursors,  $\alpha$ -cell clusters and finally  $\beta$ -cell clusters (Fig. S5F). Taken together, the Monocle2 analysis seemed to be more consistent with our current understanding of endocrine specification, and we used this method for further downstream analysis.

To focus on how fate choices are made between cells progressing towards either an  $\alpha$ - or  $\beta$ -cell fate, we performed an expression analysis on how genes are differentially regulated in both branches after the branch point. In this way, we could identify genes that are specific for either  $\alpha$ - or  $\beta$ -cell fate acquisition. Unsurprisingly, many of the top regulated genes that were identified by this analysis were genes that were already differentially expressed between  $\alpha$ - and

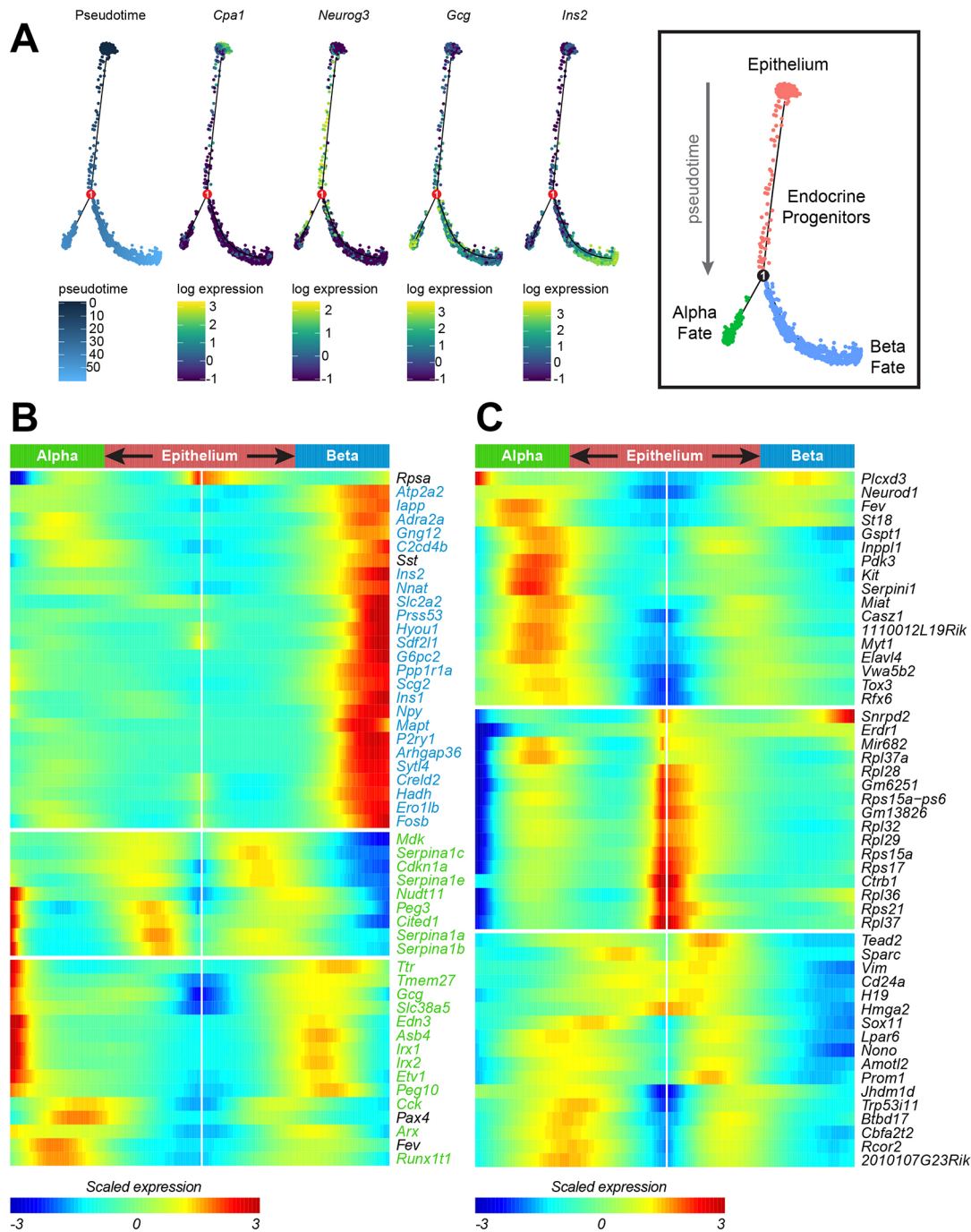


**Fig. 4. Pseudotime ordering of embryonic pancreatic cells reveals novel genes with specific regulation patterns during endocrine differentiation.**

(A) Trajectories for  $\alpha$ - and  $\beta$ -cell differentiation in the developing pancreas. Pseudotime progresses from the top through the branch point towards the bottom, as indicated by color in the first panel. Pancreatic epithelial cells are located at the top of the trajectory,  $\alpha$ -cells on the left trajectory and  $\beta$ -cells are on the right trajectory, as indicated by *Cpa1*, *Gcg* and *Ins2* expression. *Neurog3* expression indicates that endocrine progenitors are located in between these populations. (B) Branched expression analysis of the  $\alpha$ - and  $\beta$ -branches that were determined in the pseudotime analysis. The top 50 differentially regulated genes are hierarchically clustered into three groups. The start of pseudotime, in the ductal epithelium, is located in the middle and extends to the left for the  $\alpha$ -branch, and to the right for the  $\beta$ -branch. Color indicates scaled expression, from  $-3$  (blue) to  $+3$  (red). Gene names are color-coded for overlap with  $\alpha$ -cell identity genes (green) or  $\beta$ -cell identity genes (blue). (C) Branched expression analysis of the  $\alpha$ - and  $\beta$ -branches that were determined in the pseudotime analysis. The top 50 differentially regulated genes after removal of  $\alpha$ - and  $\beta$ -identity genes are hierarchically clustered into three groups. Color indicates scaled expression, from  $-3$  (blue) to  $+3$  (red). Gene names are color-coded for overlap with  $\alpha$ -cell identity genes (green) or  $\beta$ -cell identity genes (blue).

$\beta$ -cells (Fig. 4B), like *Ins2*, *Iapp*, *Npy*, *Hadh* and *G6pc2* in the  $\beta$ -cell branch and *Gcg*, *Arx*, *Irx2* and *Ttr* in the  $\alpha$ -cell branch. We then removed all genes from our branched expression analysis that intersected with genes that were differentially expressed between clusters 8 and 9 ( $\alpha$ -cell fate) and clusters 1 and 7 ( $\beta$ -cell fate). The

remaining genes should thus represent a list of genes that are implicated in regulation of  $\alpha$ - or  $\beta$ -cell fate acquisition, without being direct markers of these cell types (Fig. 4C). A subset of these genes represent ribosomal proteins that are highly expressed in the ductal epithelium, while another subset of these genes co-express with

Neurog3-expressing endocrine progenitors, like *Serpini1* (which is associated with neuronal development; Lee et al., 2006), *Inpp1l* (which is associated with metabolic syndrome; Sleeman et al., 2005) and *Prom1* (an adult stem cell marker; Katoh et al., 2007).

### Expression patterns of combinations of genes, or individual genes in developmental time, are predictive of cell fate acquisition

Plotting gene expression in pseudotime allowed us to obtain the directionality of gene expression throughout pancreatic development. Thus, we investigated how gene expression signatures changed during the major transitions through pseudotime in our dataset. First, we plotted the imputed expression of known markers *Cpa1*, *Sox9*, *Gcg* and *Ins2* (Fig. 5A). As expected, expression for *Cpa1* and *Sox9* was high in the epithelium, which was organized in the beginning of pseudotime (red dots). The expression for these genes markedly declined over pseudotime, and was very low in both cells with an  $\alpha$ - and  $\beta$ -cell-fate. *Gcg* and *Ins2* expression, reversely, was low in the epithelium and increased in its specific populations over pseudotime: *Gcg* markedly increased expression in  $\alpha$ -cells, whereas *Ins2* was strongly upregulated in  $\beta$ -cells. The  $\alpha$ - and  $\beta$ -cell transcription factors *Arx* and *Pdx1* showed very similar patterns to their cell type-specific hormones. *Neurog3* was not associated with a specific branch, but showed a marked and narrow peak in expression around pseudotime 20, before the data splits into the  $\alpha$  and  $\beta$  branches. *Fev*, a marker for cells in cluster 4, which we dubbed as transitory endocrine progenitors, peaks later in pseudotime than *Neurog3*, but before the hormones *Gcg* in  $\alpha$  cells and *Ins2* in  $\beta$  cells, which is also in line with expectations. Finally, we checked expression patterns of some novel markers for endocrine cells. *Amotl2* and *Btd17*, both novel endocrine progenitor markers, show the same specific and narrow expression peak as *Neurog3*. Finally, expression patterns of *Prom1* and *Hopx* were plotted as novel branch-specific endocrine progenitor fate acquisition markers for  $\alpha$ - and  $\beta$ -cells, respectively (Fig. 5A).

As combinations of expressed genes can be indicative of specific populations of cells, we sought to investigate relations between typical markers in subpopulations of our dataset. *Ptf1a* and *Sox9*, for example, are typical markers for the tip and trunk of the pancreatic epithelium, respectively. However, their co-expression indicates multipotent cells in the tip structures (Pan et al., 2013). In our data, their expression is negatively correlated (Fig. 5B), as indicated by polynomial interpolation, although most cells express both genes at some abundance. *Hes1* is a notch signal that inhibits *Neurog3* expression (Ahnfelt-Ronne et al., 2012), and thus their expression in the pancreatic epithelium is mutually exclusive, whereas the expression of trunk markers *Hes1* and *Sox9* is positively correlated (Fig. 5B).

In the endocrine differentiation of  $\alpha$ - and  $\beta$ -cells, the first stages of development (represented in clusters 5 and 4) are shared between the cell types. As a consequence, the start of the gene trajectories in pseudotime is similar. *Neurog3* expression rapidly diminishes after peaking in the beginning of pseudotime. *Pax4* and *Arx*, which are considered to be key regulators in  $\alpha$ - and  $\beta$ -cell fate decisions (Napolitano et al., 2015), are both expressed in endocrine progenitors. On a transcriptome level, *Pax4* expression gradually declines during both  $\alpha$ - and  $\beta$ -cell development, but *Arx* expression is maintained in  $\alpha$ -cells while  $\beta$ -cells downregulate *Arx* towards maturation. Interestingly, no obvious correlation was found between the expression of *Pax4* and *Arx* in endocrine progenitors, although *Pax4* expression was upregulated in *Neurog3*-expressing cluster 5 compared with the developmentally more advanced progenitor cluster 4. Finally, while *Arx* and *Gcg* are positively correlated in

developing  $\alpha$ -cells, *Pax4* and *Ins2* are negatively correlated in developing  $\beta$ -cells, which indicated that *Pax4* expression is reduced at the later stages of pseudotime in  $\beta$ -cells.

In conclusion, this dataset can be used to mine gene signatures that are co- or anti-correlated. By following the gene signatures described in Fig. 5 and using our website ([singlecellpancreas.eu](http://singlecellpancreas.eu)) to check the expression of any given gene in the embryonic pancreas, the user can obtain a better grasp of key gene expression patterns important for cell type specification during pancreatic development. This resource serves as a starting point for understanding pancreas developmental transitions at a time-resolved single cell resolution.

### DISCUSSION

In this study, we present a comprehensive dataset containing single cells from the mouse embryonic pancreas from embryonic ages E12.5 to E18.5. Although we focus on  $\alpha$ - and  $\beta$ -cell development, the dataset contains all known cell types of the developing pancreas, and allowed us to discover heterogeneity within the epithelial tip, endocrine precursors, and developing  $\alpha$ - and  $\beta$ -cells. We expect this dataset to be a valuable resource for mining genes that are lineage and cell-type restricted during pancreatic development.

We used lineage reconstruction analysis to indicate the existence of an immature endocrine state between the *Neurog3*<sup>+</sup> endocrine progenitors and the mature endocrine cell types. The gene *Fev* specifically marks this particular population, which we call transitory endocrine progenitors. This gene has been described recently in subpopulations of embryonic pancreas cells at E15.5 and E18.5 (Krentz et al., 2018). Pseudotime analysis along  $\alpha$ - and  $\beta$ -cell differentiation further reveals how cells progress from one cell state to the next in developmental time, and allows us to assess dynamic gene expression changes. Well known markers, such as *Cpa1*, *Sox9*, *Neurog3* and the hormones *Ins2* and *Gcg*, behave as expected in this pseudo-temporal timeline (Ahnfelt-Ronne et al., 2012), and clustering of all differentially regulated genes provides a resource of known and unknown genes in pancreatic development that can be harvested for potential new markers and candidate genes important for pancreatic development.

The gene *Amotl2*, for example, was found to be co-expressed with *Neurog3* in the endocrine progenitor population. This gene has been shown to be important for cell movement in zebrafish embryos (Huang et al., 2007), breaking of cell polarity and tumor invasion (Mojallal et al., 2014), as well as being involved in neural development (Proszynski et al., 2013). A possible function for this gene could be in the delamination of *Neurog3*<sup>+</sup> progenitor cells to a more endocrine-committed transitory progenitor cell state, marked by *Fev*. We postulate that finding genes like this, with no known function in pancreatic development but with described functions in other tissues can provide a good starting point for generating new hypotheses regarding pancreatic development.

Importantly, we used a MIP-GFP reporter to enrich for endocrine cells in general and  $\beta$ -cells in particular, which means that this dataset is skewed towards  $\beta$ -cell differentiation within the endocrine compartment and could have limited use when studying other lineage allocations. This enrichment specifically allowed us to build a more-complete and faithful roadmap for  $\beta$ -cells. This strategy has been used recently (Krentz et al., 2018) to achieve a similar enrichment for endocrine cells from E15.5 and E18.5 mouse embryos, showing the necessity of focusing on a particular cell type to build a complete roadmap. However, other cell types, such as  $\alpha$ -cells, are also abundantly present in the dataset, can be followed through pseudotime and are a valuable resource for the research community. We postulate that dim GFP expression driven by the

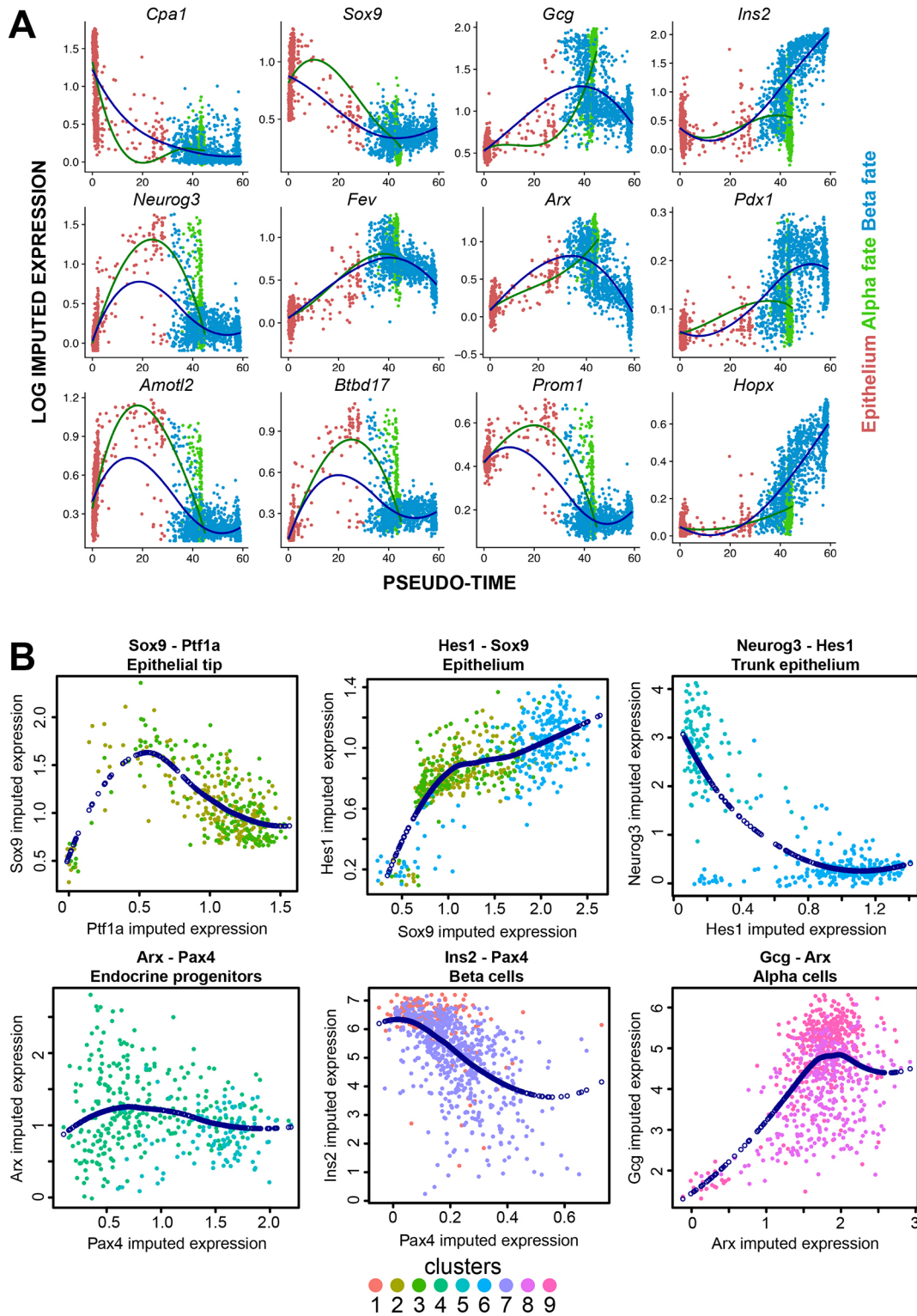


**Fig. 5. Pseudo-temporal expression patterns of key factors of pancreatic development and their interactions.** (A) Expression dynamics of specific genes in pseudotime. In each plot, log imputed expression is plotted for each cell as a function of pseudotime. Color indicates the state of the cell (epithelium in red,  $\alpha$  fate in green or  $\beta$  fate in blue). Loess curve fitting represents the local polynomial regression over pseudotime for both  $\alpha$ - and  $\beta$ -fate progression from the epithelium, indicated by color ( $\alpha$ -fate in green or  $\beta$ -fate in blue). (B) Log imputed expression of key developmental genes were plotted against each other for cells of specific clusters, as indicated in the plots, to show their relationship during specific stages of development. Colors indicate which clusters the cells belong to; dark-blue dots represent polynomial interpolations to indicate relationships between genes.

mouse insulin promoter in non- $\beta$  endocrine cells allowed us to still enrich for these cells, albeit less efficiently, thus increasing our yield of these cell types.

Other studies have been performed to characterize the embryonic pancreas at the single cell level. However, as these studies were carried out on a small subset of genes (Petersen et al., 2017), at a

single time point (E13.5) (Stanescu et al., 2017) or with limited sequencing depth (QC threshold of 200 genes per cell) (Byrnes et al., 2018), they are of limited use when following gene expression changes during the second transition in pancreatic development. We therefore decided to build on these datasets by making a comprehensive roadmap containing cells from several embryonic ages (E12.5, E13.5, E14.5, E15.5 and E18.5), combined with high-depth sequencing (median over 5000 genes per cell). We show that this dataset can be mined for novel marker genes, to study cell type heterogeneity and to find gene expression patterns that play a role in forming the different cell types that make up the pancreas, especially those of  $\alpha$ - and  $\beta$ -cells, which were the focus of this study. We hope this study, which can be browsed at [singlecellpancreas.eu](http://singlecellpancreas.eu), will provide a valuable resource for understanding pancreatic development.

## MATERIALS AND METHODS

### Animal experiments

Mouse embryos that express GFP under transcriptional control of the mouse insulin promoter (MIP-GFP mice, Jackson Laboratories #006864) were isolated at embryonic days (E) 12.5, E13.5, E14.5, E15.5 and E18.5. All experiments on animals were carried out in accordance with the guidelines of the Animal Welfare Committee of the Royal Netherlands Academy of Arts and Sciences (KNAW).

### Tissue preparation

From obtained embryos, the pancreas was isolated as described previously (Petzold and Spagnoli, 2012). Pancreases from MIP-GFP embryos were digested into single cells using TrypLE (Thermo Fisher, #12605010) containing 10  $\mu$ g/ml pulmozyme (Roche, Basel, Switzerland), and washed with PBS containing 10% FBS (Thermo Fisher, 10500064). Cells were stored on ice until they were sorted using FACS. DAPI (Thermo Fisher, D1306, 20  $\mu$ g/ml) or TO-PRO3 (Thermo Fisher, T3605, 1  $\mu$ M) was added to cell suspensions immediately before sorting to distinguish between live and dead cells.

### FACS sorting

Cells were sorted as single cells into hard-shell 384-well PCR plates (BioRad) containing 100 or 200 nl of RT primers, dNTPs (Promega), ERCC spike-ins (Ambion) and 5  $\mu$ l vapor-lock (Qiagen) using FACSJazz or FACSARIA II (BD biosciences) as described previously (Muraro et al., 2016). For every embryonic age, MIP-GFP-negative cells as well as MIP-GFP-positive cells (to enrich for endocrine cell types) were sorted into separate plates (Fig. S1A). Index sorting was performed in order to couple FACS-obtained data such as forward scatter, side scatter and GFP intensity to our transcriptome data. Sorted cells in plates were snap frozen on dry ice and stored at  $-80^{\circ}\text{C}$ .

### Processing of sorted cells

Plates of sorted cells were thawed on ice and lysed at  $65^{\circ}\text{C}$ , after which reverse transcription (RT) and second-strand reactions were carried out. RT reactions were performed using primers containing a polyT tail, a 4 or 6 bp unique molecular identifier (UMI) sequence, a cell-specific barcode sequence (8 bp), an Illumina 5' adapter and a T7 promoter sequence. Contents from all wells in a plate were pooled into a single library after second-strand synthesis. RNA in these libraries underwent linear amplification using *in vitro* transcription, followed by fragmentation to lengths between 200 and 1000 bp. Next, a second RT reaction using random hexamer primers containing the Illumina 3' adapter was performed and libraries were amplified using PCR. Sequencing was performed on Illumina NextSeq (paired-end, 75 bp reads). A median of 90,000 reads per cell were sequenced.

### Library sequencing and mapping

Sequenced reads were mapped to a reference transcriptome based on the mouse genome release mm10 as described previously (Muraro et al., 2016). Reads with the same UMI – barcode – transcript combination were likely

caused by PCR over-amplification and were thus counted as a single read, and the number of reads per transcript per cell were corrected for RNA – UMI collision using poissonian counting statistics (Grün et al., 2015). Data from all plates were pooled into a single dataset containing 7296 cells and 19,788 genes.

### Data processing

Cells with fewer than 6000 UMI counts and/or cells that expressed fewer than 2000 genes were filtered from the dataset. Data were processed in R using Seurat version 2.3.4 as follows: metadata were added regarding the origin of the cell (experimental code, embryonic age, live or GFP sorted). Then data were log-normalized with a scaling factor of 10,000. Variable genes were detected using an  $x$  low cut-off of 0.2 and a  $y$  low cut-off of 0.5, with high cut-offs set to infinity and data divided into 20 bins. All genes were scaled using a negative binomial model assuming UMI data, with the number of expressed UMIs and genes per cell were used as variables to regress. A total of 40 principal components were calculated and assessed using jackstraw. All PCs were found to contribute significantly and were thus used for downstream analysis. Clustering was performed using Seurat's *FindClusters* function with sensitivities ranging from 0.1 to 2 in 0.1 steps. Using *clustree* version 0.3.0, it was first observed on a sensitivity resolution of 0.5 that clustering was not changed at a higher sensitivity, and this sensitivity was then picked for assessment of clustering using the *AssessNodes* function of Seurat after building a clustering tree of the clustering. Nodes that had a higher out-of-bag error rate than 10% were removed and clusters underneath these nodes were merged. UMAP dimensional reduction was calculated using the *umap* package version 0.1.0.3, with metric function set to euclidean and using only variable genes, as detected by Seurat. Differential expression was calculated between clusters using the *FindMarkers* function from Seurat, using the 'negbinom' test, and the number of expressed UMIs and genes per cell were used as variables to regress. Based on the top upregulated genes per cluster, cell type identities were determined for each cluster and clusters that represent the same cell type were merged. Differential expression for individual cell types was then calculated similarly as it was calculated for clusters.

Next, cells expressing more than three raw UMI counts of *ApoE* or *Cd93*, or five transcripts *Coll1a1* or *Hbb-y* were excluded from the dataset, as they represented cell populations unrelated to endocrine or exocrine cells (blood vessel, immune, mesenchyme and red blood cells). The genes *Malat1*, *Lars2* and *Rn45s*, which were strongly upregulated in some libraries and are linked to cellular stress (Yao et al., 2016; Schild et al., 2014; Yoshikawa and Fujii, 2016), were then excluded from the dataset. After filtering, the full dataset consisted of 2589 cells and 19,696 genes. To correct for any batch effects caused by the embryonic age of the collected tissues, Seurat objects were then generated per embryonic age, and data were log-normalized and scaled as described previously. Cells from different embryonic ages were then merged into a single dataset using *multiCCA* (Butler et al., 2018), using the first six CCAs for downstream analysis. Experiment identifiers, embryonic age and FACS characteristics were added manually to metadata. Cell cycle state was calculated as described previously (Tirosh et al., 2016). Clustering resolution was set to 0.7 and was consecutively evaluated using Seurat's *AssessNodes* function. Clusters were merged when the out-of-box error scores were above 10%. In this manuscript, pancreatic epithelium is defined as the cells from the tip and trunk domain. Differentially expressed genes per cluster, and differential expression between specific clusters, was calculated using the *FindMarkers* function in Seurat using the 'negbinom' test, with the number of genes and UMIs for every cell as variables to regress. Data for specific genes (*Cpa1*, *Ptf1a*, *Sox9*, *Hes1*, *Gcg*, *Ins2*, *Neurog3*, *Fev*, *Arx*, *Pax4*, *Pdx1*, *Amotl2*, *Btd17*, *Prom1* and *Hopx*) was imputed using the *AddImputedScore* function of Seurat, using all variable genes as template to fit. Imputed data was only used to generate comparative gene plots. To determine which cells can be designated to express a hormone, density plots were generated for the hormones of all cells. For *Gcg*- and *Ins2*-expressing cells, bimodal expression patterns could clearly be observed, and the local minimum between the modes was mathematically determined (4.23 log-normalized counts for *Gcg*, 4.16 log-normalized counts for *Ins2*). For  $\gamma$ - and  $\delta$ -cells, a

bimodal expression distribution was not found, owing to the low number of *Ppy*- and *Sst*-expressing cells. As a compromise, we decided that any cell that expressed any hormone with more than four log-normalized counts was considered to be a hormone-expressing cell for that hormone. If a cell passed the threshold for more than one hormone, we considered it to be poly-hormonal. Hormone expression signatures per cell were then added to the metadata.

### Pseudotime analysis

Raw data were filtered so that the same cells and genes remained as for the Seurat object containing only the pancreatic epithelial endocrine cells, and was then used in the single cell RNA-sequencing toolkit Monocle2 version 2.10.1 (Qiu et al., 2017b,c). Clustering information from Seurat was transferred to the monocle pData object. Differential expression was calculated using the *differentialGeneTest* from Monocle, using the Seurat-determined clusters to generate a full model. Genes that had a q-value lower than 0.05 were used to set the ordering filter and reduce dimensions using DDRTree version 0.1.5. Differentially regulated genes in pseudotime were calculated using full model '~sm.ns(Pseudotime)', and genes that were differentially regulated between the  $\alpha$  and  $\beta$  branch were calculated using the *BEAM* function in monocle. The top 50 differentially regulated genes, as determined by BEAM, were clustered into three groups using ward.D2 as clustering method. Genes were then removed that were differentially expressed between  $\alpha$ - and  $\beta$ -cells, as determined by Seurat (clusters 1+7 versus cluster 8+9, *FindMarkers* function using 'negbinom' test and regressing the number of UMIs and genes). The top 50 remaining differentially regulated genes from the BEAM analysis were then also clustered into three groups using ward.D2.

### Pathway analysis

Gene ontology was performed using the web interface www.geneontology.org. Only biological processes for *Mus musculus* were obtained this way. For gene-set enrichment analysis (GSEA), the GSEA Java Desktop Application from the BROAD institute was used (software.broadinstitute.org/gsea/index.jsp) and GSEA was calculated using h.all, c1.all, c2.all, c3.all, c4.all, c5.all, c6.all and c7.all geneset databases.

### Software and resources

Rstudio version 1.1.463 was used in combination with R version 3.5.3. Data were processed using Seurat version 2.3.4 (Butler et al., 2018) and Monocle version 2.10.1 (Qiu et al., 2017b,c). Clustering was assessed using clustree version 0.3.0.

### Acknowledgements

We thank Céline Ziegler-Birling for technical assistance.

### Competing interests

The authors declare no competing or financial interests.

### Author contributions

Conceptualization: L.v.G., E.J.P.d.K.; Methodology: L.v.G., M.J.M., E.J.P.d.K.; Software: L.v.G., M.J.M.; Validation: G.D.; Formal analysis: L.v.G., M.J.M.; Investigation: L.v.G., M.J.M., T.D., L.S.; Resources: M.J.M., G.G., A.v.O., E.J.P.d.K.; Data curation: L.v.G., M.J.M.; Writing - original draft: L.v.G., M.J.M., G.D., G.G., E.J.P.d.K.; Visualization: L.v.G.; Supervision: A.v.O., E.J.P.d.K.; Project administration: A.v.O., E.J.P.d.K.; Funding acquisition: A.v.O., E.J.P.d.K.

### Funding

Financial support was provided by the Diabetes Fonds, by Stichting Diabetes Onderzoek Nederland and by the Tjanka Foundation. The Gerard Gradwohl lab is supported by a Challenge Grant from the Novo Nordisk Fonden (NNF14SA0005).

### Data availability

The single-cell sequencing data described in this study have been deposited in GEO under accession number GSE132364.

### Supplementary information

Supplementary information available online at <http://dev.biologists.org/lookup/doi/10.1242/dev.173716.supplemental>

### References

- Ahnfelt-Ronne, J., Jorgensen, M. C., Klinck, R., Jensen, J. N., Fuchtbauer, E.-M., Deering, T., Macdonald, R. J., Wright, C. V. E., Madsen, O. D. and Serup, P. (2012). Ptf1a-mediated control of Dll1 reveals an alternative to the lateral inhibition mechanism. *Development* **139**, 33-45. doi:10.1242/dev.071761
- Baron, M., Veres, A., Wolock, S. L., Faust, A. L., Gaujoux, R., Vetere, A., Ryu, J. H., Wagner, B. K., Shen-Orr, S. S., Klein, A. M. et al. (2016). A single-cell transcriptomic map of the human and mouse pancreas reveals inter- and intra-cell population structure. *Cell Syst.* **3**, 346-360.e4. doi:10.1016/j.cels.2016.08.011
- Butler, A., Hoffman, P., Smibert, P., Papalexi, E. and Satija, R. (2018). Integrating single-cell transcriptomic data across different conditions, technologies, and species. *Nat. Biotechnol.* **36**, 411-420. doi:10.1038/nbt.4096
- Byrnes, L. E., Wong, D. M., Subramaniam, M., Meyer, N. P., Gilchrist, C. L., Knox, S. M., Tward, A. D., Ye, C. J. and Sneddon, J. B. (2018). Lineage dynamics of murine pancreatic development at single-cell resolution. *Nat. Commun.* **9**, 3922. doi:10.1038/s41467-018-06176-3
- Collombat, P., Mansouri, A., Hecksher-Sorensen, J., Serup, P., Krull, J., Gradwohl, G. and Gruss, P. (2003). Opposing actions of Arx and Pax4 in endocrine pancreas development. *Genes Dev.* **17**, 2591-2603. doi:10.1101/gad.269003
- Collombat, P., Hecksher-Sørensen, J., Broccoli, V., Krull, J., Ponte, I., Mundiger, T., Smith, J., Gruss, P., Serup, P. and Mansouri, A. (2005). The simultaneous loss of Arx and Pax4 genes promotes a somatostatin-producing cell fate specification at the expense of the alpha- and beta-cell lineages in the mouse endocrine pancreas. *Development* **132**, 2969-2980. doi:10.1242/dev.01870
- De Vas, M. G., Kopp, J. L., Heliot, C., Sander, M., Cereghini, S. and Haumaitre, C. (2015). Hnf1b controls pancreas morphogenesis and the generation of Ngn3+ endocrine progenitors. *Development* **142**, 871-882. doi:10.1242/dev.110759
- Fang, Z., Weng, C., Li, H., Tao, R., Mai, W., Liu, X., Lu, L., Lai, S., Duen, Q., Alvarez, C. et al. (2019). Single-cell heterogeneity analysis and CRISPR screen identify key  $\beta$ -cell-specific disease genes. *Cell Rep.* **26**, P3132-3144.E7. doi:10.1016/j.celrep.2019.02.043
- Grapin-Botton, A., Seymour, P. A. and Gradwohl, G. (2015). Pairing-up SOX to kick-start beta cell genesis. *Diabetologia* **58**, 859-861. doi:10.1007/s00125-015-3539-2
- Grün, D. and Van Oudenaarden, A. (2015). Design and analysis of single-cell sequencing experiments. *Cell* **163**, 799-810. doi:10.1016/j.cell.2015.10.039
- Grün, D., Lyubimova, A., Kester, L., Wiebrands, K., Basak, O., Sasaki, N., Clevers, H. and Van Oudenaarden, A. (2015). Single-cell messenger RNA sequencing reveals rare intestinal cell types. *Nature* **525**, 251-255. doi:10.1038/nature14966
- Gu, G., Dubauskaite, J. and Melton, D. A. (2002). Direct evidence for the pancreatic lineage: NGN3+ cells are islet progenitors and are distinct from duct progenitors. *Development* **129**, 2447-2457.
- Huang, H., Lu, F.-I., Jia, S., Meng, S., Cao, Y., Wang, Y., Ma, W., Yin, K., Wen, Z., Peng, J. et al. (2007). Amotl2 is essential for cell movements in zebrafish embryo and regulates c-Src translocation. *Development* **134**, 979-988. doi:10.1242/dev.02782
- Imai, Y., Patel, H. R., Hawkins, E. J., Doliba, N. M., Matschinsky, F. M. and Ahima, R. S. (2007). Insulin secretion is increased in pancreatic islets of neuropeptide Y-deficient mice. *Endocrinology* **148**, 5716-5723. doi:10.1210/en.2007-0404
- Johansson, K. A., Dursun, U., Jordan, N., Gu, G., Beermann, F., Gradwohl, G. and Grapin-Botton, A. (2007). Temporal control of Neurogenin3 activity in pancreas progenitors reveals competence windows for the generation of different endocrine cell types. *Dev. Cell* **12**, 457-465. doi:10.1016/j.devcel.2007.02.010
- Katoh, Y. and Katoh, M. (2007). Comparative genomics on PROM1 gene encoding stem cell marker CD133. *Int. J. Mol. Med.* **19**, 967-970. doi:10.3892/ijmm.19.6.967
- Kim, Y. H., Larsen, H. L., Rué, P., Lemaire, L. A., Ferrer, J. and Grapin-Botton, A. (2015). Cell cycle-dependent differentiation dynamics balances growth and endocrine differentiation in the pancreas. *PLoS Biol.* **13**, e1002111. doi:10.1371/journal.pbio.1002111
- Kolodziejczyk, A. A., Kim, J. K., Svensson, V., Marioni, J. C. and Teichmann, S. A. (2015). The technology and biology of single-cell RNA sequencing. *Mol. Cell* **58**, 610-620. doi:10.1016/j.molcel.2015.04.005
- Kowalczyk, M. S., Tirosh, I., Heckl, D., Rao, T. N., Dixit, A., Haas, B. J., Schneider, R. K., Wagers, A. J., Ebert, B. L. and Regev, A. (2015). Single-cell RNA-seq reveals changes in cell cycle and differentiation programs upon aging of hematopoietic stem cells. *Genome Res.* **25**, 1860-1872. doi:10.1101/gr.192237.115
- Krentz, N. A. J., Van Hoof, D., Li, Z., Watanabe, A., Tang, M., Nian, C., German, M. S. and Lynn, F. C. (2017). Phosphorylation of NEUROG3 links endocrine differentiation to the cell cycle in pancreatic progenitors. *Dev. Cell* **41**, 129-142.e6. doi:10.1016/j.devcel.2017.02.006
- Krentz, N. A. J., Lee, M. Y. Y., Xu, E. E., Sproull, S. L. J., Maslova, A., Sasaki, S. and Lynn, F. C. (2018). Single-cell transcriptome profiling of mouse and hESC-derived pancreatic progenitors. *Stem Cell Rep.* **11**, 1551-1564. doi:10.1016/j.stemcr.2018.11.008

- Larsen, H. L., Martín-Coll, L., Nielsen, A. V., Wright, C. V. E., Trusina, A., Kim, Y. H. and Grapin-Botton, A. (2017). Stochastic priming and spatial cues orchestrate heterogeneous clonal contribution to mouse pancreas organogenesis. *Nat. Commun.* **8**, 605. doi:10.1038/s41467-017-00258-4
- Lawlor, N., George, J., Bolisetti, M., Kursawe, R., Sun, L., Sivakamasundari, V., Kycia, I., Robson, P. and Stitzel, M. L. (2017). Single-cell transcriptomes identify human islet cell signatures and reveal cell-type-specific expression changes in type 2 diabetes. *Genome Res.* **27**, 208-222. doi:10.1101/gr.212720.116
- Lee, M. S., Jun, D.-H., Hwang, C.-I., Park, S. S., Kang, J. J., Park, H.-S., Kim, J., Kim, J. H., Seo, J.-S. and Park, W.-Y. (2006). Selection of neural differentiation-specific genes by comparing profiles of random differentiation. *Stem Cells.* **24**, 1946-1955. doi:10.1634/stemcells.2005-0325
- Li, J., Klughammer, J., Farlik, M., Penz, T., Spittler, A., Barbieux, C., Berishvili, E., Bock, C. and Kubicek, S. (2016). Single-cell transcriptomes reveal characteristic features of human pancreatic islet cell types. *EMBO Rep.* **17**, 178-187. doi:10.15252/embr.201540946
- Magenheim, J., Klein, A. M., Stanger, B. Z., Ashery-Padan, R., Sosa-Pineda, B., Gu, G. and Dor, Y. (2011). Ngn3(+) endocrine progenitor cells control the fate and morphogenesis of pancreatic ductal epithelium. *Dev. Biol.* **359**, 26-36. doi:10.1016/j.ydbio.2011.08.006
- Marty-Santos, L. and Cleaver, O. (2016). Pdx1 regulates pancreas tubulogenesis and E-cadherin expression. *Development* **143**, 101-112. doi:10.1242/dev.126755
- Mcgrath, P. S., Watson, C. L., Ingram, C., Helmuth, M. A. and Wells, J. M. (2015). The basic helix-loop-helix transcription factor NEUROG3 is required for development of the human endocrine pancreas. *Diabetes* **64**, 2497-2505. doi:10.2337/db14-1412
- Miyatsuka, T., Kosaka, Y., Kim, H. and German, M. S. (2011). Neurogenin3 inhibits proliferation in endocrine progenitors by inducing Cdkn1a. *Proc. Natl. Acad. Sci. USA* **108**, 185-190. doi:10.1073/pnas.1004842108
- Mojallal, M., Zheng, Y., Hultin, S., Audebert, S., Van Harn, T., Johnsson, P., Lenander, C., Fritz, N., Mieth, C., Corcoran, M. et al. (2014). AmotL2 disrupts apical-basal cell polarity and promotes tumour invasion. *Nat. Commun.* **5**, 4557. doi:10.1038/ncomms5557
- Muraro, M. J., Dharmadhikari, G., Grün, D., Groen, N., Dielen, T., Jansen, E., Van Gurp, L., Engelse, M. A., Carlotti, F., De Koning, E. J. P. et al. (2016). A single-cell transcriptome atlas of the human pancreas. *Cell Syst.* **3**, 385-394.e3. doi:10.1016/j.cels.2016.09.002
- Napolitano, T., Avolio, F., Courtney, M., Vieira, A., Druelle, N., Ben-Othman, N., Hadzic, B., Navarro, S. and Collobat, P. (2015). Pax4 acts as a key player in pancreas development and plasticity. *Semin. Cell Dev. Biol.* **44**, 107-114. doi:10.1016/j.semcdb.2015.08.013
- Pan, F. C. and Wright, C. (2011). Pancreas organogenesis: from bud to plexus to gland. *Dev. Dyn.* **240**, 530-565. doi:10.1002/dvdy.22584
- Pan, F. C., Bankaitis, E. D., Boyer, D., Xu, X., Van De Castele, M., Magnuson, M. A., Heimberg, H. and Wright, C. V. E. (2013). Spatiotemporal patterns of multipotentiality in Ptf1a-expressing cells during pancreas organogenesis and injury-induced facultative restoration. *Development* **140**, 751-764. doi:10.1242/dev.090159
- Petersen, M. B. K., Azad, A., Ingvorsen, C., Hess, K., Hansson, M., Grapin-Botton, A. and Honoré, C. (2017). Single-cell gene expression analysis of a human ESC model of pancreatic endocrine development reveals different paths to beta-cell differentiation. *Stem Cell Rep.* **9**, 1246-1261. doi:10.1016/j.stemcr.2017.08.009
- Petzold, K. M. and Spagnoli, F. M. (2012). A system for ex vivo culturing of embryonic pancreas. *J. Vis. Exp.* e3979. doi:10.3791/3979
- Pound, L. D., Oeser, J. K., O'Brien, T. P., Wang, Y., Faulman, C. J., Dadi, P. K., Jacobson, D. A., Hutton, J. C., Mcguinness, O. P., Shiota, M. et al. (2013). G6PC2: a negative regulator of basal glucose-stimulated insulin secretion. *Diabetes* **62**, 1547-1556. doi:10.2337/db12-1067
- Proszynski, T. J. and Sanes, J. R. (2013). Amotl2 interacts with LL5 $\beta$ , localizes to podosomes and regulates postsynaptic differentiation in muscle. *J. Cell Sci.* **126**, 2225-2235. doi:10.1242/jcs.121327
- Qiu, W.-L., Zhang, Y.-W., Feng, Y., Li, L.-C., Yang, L. and Xu, C.-R. (2017a). Deciphering pancreatic islet  $\beta$  cell and  $\alpha$  cell maturation pathways and characteristic features at the single-cell level. *Cell Metab.* **25**, 1194-1205.e4. doi:10.1016/j.cmet.2017.04.003
- Qiu, X., Mao, Q., Tang, Y., Wang, L., Chawla, R., Pliner, H. A. and Trapnell, C. (2017b). Reversed graph embedding resolves complex single-cell trajectories. *Nat. Methods* **14**, 979-982. doi:10.1038/nmeth.4402
- Qiu, X., Hill, A., Packer, J., Lin, D., Ma, Y.-A. and Trapnell, C. (2017c). Single-cell mRNA quantification and differential analysis with Census. *Nat. Methods* **14**, 309-315. doi:10.1038/nmeth.4150
- Schild, C., Hahn, D., Schaller, A., Jackson, C. B., Rothen-Rutishauser, B., Mirkovitch, J. and Nuoffer, J.-M. (2014). Mitochondrial leucine tRNA level and PTC1 are regulated in response to leucine starvation. *Amino Acids* **46**, 1775-1783. doi:10.1007/s00726-014-1730-2
- Schnuriger, A., Dominguez, S., Guiguet, M., Harfouch, S., Samri, A., Ouazene, Z., Slama, L., Simon, A., Valantin, M.-A., Thibault, V. et al. (2009). Acute hepatitis C in HIV-infected patients: rare spontaneous clearance correlates with weak memory CD4 T-cell responses to hepatitis C virus. *AIDS* **23**, 2079-2089. doi:10.1097/QAD.0b013e328330ed24
- Segerstolpe, A., Palasantza, A., Eliasson, P., Andersson, E.-M., Andréasson, A.-C., Sun, X., Picelli, S., Sabirsh, A., Clausen, M., Bjursell, M. K. et al. (2016). Single-cell transcriptome profiling of human pancreatic islets in health and type 2 diabetes. *Cell Metab.* **24**, 593-607. doi:10.1016/j.cmet.2016.08.020
- Seymour, P. A., Freude, K. K., Tran, M. N., Mayes, E. E., Jensen, J., Kist, R., Scherer, G. and Sander, M. (2007). SOX9 is required for maintenance of the pancreatic progenitor cell pool. *Proc. Natl. Acad. Sci. USA* **104**, 1865-1870. doi:10.1073/pnas.0609217104
- Shih, H. P., Kopp, J. L., Sandhu, M., Dubois, C. L., Seymour, P. A., Grapin-Botton, A. and Sander, M. (2012). A Notch-dependent molecular circuitry initiates pancreatic endocrine and ductal cell differentiation. *Development* **139**, 2488-2499. doi:10.1242/dev.078634
- Sleeman, M. W., Wortley, K. E., Lai, K.-M. V., Gowen, L. C., Kintner, J., Kline, W. O., Garcia, K., Stitt, T. N., Yancopoulos, G. D., Wiegand, S. J. et al. (2005). Absence of the lipid phosphatase SHIP2 confers resistance to dietary obesity. *Nat. Med.* **11**, 199-205. doi:10.1038/nm1178
- Sosa-Pineda, B., Chowdhury, K., Torres, M., Oliver, G. and Gruss, P. (1997). The Pax4 gene is essential for differentiation of insulin-producing beta cells in the mammalian pancreas. *Nature* **386**, 399-402. doi:10.1038/386399a0
- Stanescu, D. E., Yu, R., Won, K.-J. and Stoffers, D. A. (2017). Single cell transcriptomic profiling of mouse pancreatic progenitors. *Physiol. Genomics* **49**, 105-114. doi:10.1152/physiolgenomics.001114.2016
- Street, K., Rizzo, D., Fletcher, R. B., Das, D., Ngai, J., Yosef, N., Purdom, E. and Dudoit, S. (2018). Slingshot: cell lineage and pseudotime inference for single-cell transcriptomics. *BMC Genomics* **19**, 477. doi:10.1186/s12864-018-4772-0
- Tirosh, I., Izar, B., Prakadan, S. M., Wadsworth, M. H., Treacy, D., Trombetta, J. J., Rotem, A., Rodman, C., Lian, C., Murphy, G. et al. (2016). Dissecting the multicellular ecosystem of metastatic melanoma by single-cell RNA-seq. *Science* **352**, 189-196. doi:10.1126/science.aad0501
- Veres, A., Faust, A. L., Bushnell, H. L., Engquist, E. N., Kenty, J. H.-R., Harb, G., Poh, Y.-C., Sintov, E., Gürtler, M., Paggiuca, F. W., Peterson, Q. P., Melton, D. A. (2019). Charting cellular identity during human in vitro  $\beta$ -cell differentiation. *Nature* **569**, 368-373. doi:10.1038/s41586-019-1168-5
- Wang, Y. J., Schug, J., Won, K.-J., Liu, C., Najji, A., Avrahami, D., Golson, M. L. and Kaestner, K. H. (2016). Single-Cell Transcriptomics of the Human Endocrine Pancreas. *Diabetes* **65**, 3028-3038. doi:10.2337/db16-0405
- Xin, Y., Dominguez Gutierrez, G., Okamoto, H., Kim, J., Lee, A.-H., Adler, C., Ni, M., Yancopoulos, G. D., Murphy, A. J. and Gromada, J. (2018). Pseudotime ordering of single human  $\beta$ -cells reveals states of insulin production and unfolded protein response. *Diabetes* **67**, 1783-1794. doi:10.2337/db18-0365
- Xin, Y., Kim, J., Okamoto, H., Ni, M., Wei, Y., Adler, C., Murphy, A. J., Yancopoulos, G. D., Lin, C., Gromada, J. et al. (2016). RNA sequencing of single human islet cells reveals type 2 diabetes genes. *Cell Metab.* **24**, 608-615. doi:10.1016/j.cmet.2016.08.018
- Yao, J., Wang, X. Q., Li, Y. J., Shan, K., Yang, H., Wang, Y. N. Z., Yao, M. D., Liu, C., Li, X. M., Shen, Y. et al. (2016). Long non-coding RNA MALAT1 regulates retinal neurodegeneration through CREB signaling. *EMBO Mol. Med.* **8**, 1113. doi:10.15252/emmm.201606749
- Yoshikawa, M. and Fujii, Y. R. (2016). Human ribosomal RNA-derived resident microRNAs as the transmitter of information upon the cytoplasmic cancer stress. *Biomed. Res. Int.* **2016**, 7562085. doi:10.1155/2016/7562085
- Zhou, Q., Law, A. C., Rajagopal, J., Anderson, W. J., Gray, P. A. and Melton, D. A. (2007). A multipotent progenitor domain guides pancreatic organogenesis. *Dev. Cell* **13**, 103-114. doi:10.1016/j.devcel.2007.06.001